Inorg. Chem. **2003**, *42*, 6812–6823

Iron Nitrosyls of a Pentadentate Ligand Containing a Single Carboxamide Group: Syntheses, Structures, Electronic Properties, and Photolability of NO

Apurba K. Patra,[†] John M. Rowland,[†] Dana S. Marlin,[‡] Eckhard Bill,[‡] Marilyn M. Olmstead,[§] and Pradip K. Mascharak*,[†]

Department of Chemistry and Biochemistry, University of California, Santa Cruz, California 95064, Department of Chemistry, University of California, Davis, California 95616, and Max-Plank-Institut für Strahlenchemie, Stiftstrasse 34-36, D-45470 Mülheim an der Ruhr, Germany

Received May 16, 2003

Three iron complexes of a pentadentate ligand *N*,*N*-bis(2-pyridylmethyl)amine-*N*-ethyl-2-pyridine-2-carboxamide ($PaPy_3H$, H is the dissociable amide proton) have been synthesized. All three species, namely, two nitrosyls $[(PaPy_3)Fe(NO)](ClO_4)_2$ (**2**) and $[(PaPy_3)Fe(NO)](ClO_4)$ (**3**) and one nitro complex $[(PaPy_3)Fe(NO_2)](ClO_4)$ (**4**), have been structurally characterized. These complexes provide the opportunity to compare the structural and spectral properties of a set of isostructural $\{Fe–NO\}^{6,7}$ complexes (**2** and **3**, respectively) and an analogous genuine Fe(III) complex with an "innocent" sixth ligand ($[(PaPy_3)Fe(NO_2)](ClO_4)$, **4**). The most striking difference in the structural features of **2** and **3** is the Fe–N–O angle (Fe–N–O = 173.1(2)° in the case of **2** and 141.29(15)° in the case of **3**). The clean ^1H NMR spectrum of **2** in CD_3CN reveals its $S = 0$ ground state and confirms its $\{Fe–NO\}^6$ configuration. The binding of NO at the non-heme iron center in **2** is *completely reversible* and the bound NO is *photolabile*. Mössbauer data, electron paramagnetic resonance signal at $g \approx 2.00$, and variable temperature magnetic susceptibility measurements indicate the $S = {}^1/_2$ spin state of the $\{Fe–NO\}^7$ complex **3**. Analysis of the spectroscopic data suggests $Fe(II)–NO^+$ and $Fe(II)–NO^•$ formulations for **2** and **3**, respectively. The bound NO in **3** does not show any photolability. However, in MeCN solution, it reacts rapidly with dioxygen to afford the nitro complex **4**, which has also been synthesized independently from $[(PaPy_3)Fe(MeCN)]^{2+}$ and NO_2^-. Nucleophilic attack of hydroxide ion to the N atom of the NO ligand in **2** in MeCN in the dark gives rise to **4** in high yield.

Introduction

Syntheses of metal complexes with bound nitric oxide (NO), commonly known as metal nitrosyls, and studies on the electronic, structural, and reactivity parameters of metal-bound NO group(s) have raised great interests since the early days of coordination chemistry.[1] In recent years, interest in metal nitrosyl complexes has been renewed following the successful use of sodium nitroprusside as a NO-donor drug to control blood pressure.[2] Indeed, NO complexes that release nitric oxide (NO) upon illumination have been used as agents in photodynamic therapy (PDT).[3] Since NO has been identified as a key neurotransmitter and mammalian bio-regulator,[4] complexes that release NO under specific physiological conditions have been sought for drug use. Binding of NO to metalloenzymes has also been studied quite extensively in recent years. NO binds to the Fe(II) site of both heme[5] and non-heme iron enzymes.[6] It also binds

* Author to whom correspondence should be addressed. E-mail: mascharak@chemistry.ucsc.edu.
[†] University of California, Santa Cruz.
[‡] Max-Plank-Institut für Strahlenchemie.
[§] University of California, Davis.

(1) Richter-Addo, G. B.; Legzdins, P. *Metal Nitrosyls*; Oxford University Press: New York, 1992.
(2) (a) Clarke, M. J.; Gaul, J. B. *Struct. Bonding* (*Berlin*) **1993**, *81*, 147. (b) Butler, A. R.; Williams, D. L. H. *Chem. Soc. Rev.* **1993**, *22*, 223.
(3) (a) Ackroyd, R.; Kelty, C.; Brown, N.; Reed, M. *Photochem. Photobiol.* **2001**, *74*, 656. (b) Pandey, R. K. *J. Porphyrins Phthalocyanines* **2000**, *4*, 368.
(4) (a) Murad, F. *Angew. Chem., Int. Ed. Engl.* **1999**, *38*, 1856. (b) Ignarro, L. J. *Angew. Chem., Int. Ed. Engl.* **1999**, *38*, 1882. (c) *Methods in Nitric Oxide Research*; Feelish, M., Stamler, J. S., Eds. Wiley: Chichester, UK, 1996. (d) Feldman, P. L.; Griffith, O. W.; Stuehr, D. J. *Chem. Eng. News* **1993**, *71*, 26. (e) Culotta, E.; Koshland, D. E. *Science* **1992**, *258*, 1862. (f) Moncada, S.; Palmer, R. M. J.; Higgs, E. A. *Pharmacol. Rev.* **1991**, *43*, 109.

10.1021/ic0301627 CCC: $25.00
Published on Web 09/16/2003

reversibly to the non-heme Fe(III) site of the enzyme nitrile hydratase (NHase).[7]

Since both the metal center and the NO ligand can accept or lose electron(s), the correct assignments of the oxidation and spin states of the metal centers in metal nitrosyls as well as NO-bound Fe sites in proteins remain somewhat ambiguous. Enemark and Feltham have introduced a $\{M-NO\}^n$ notation to describe the bonding in metal nitrosyls where n represents the sum of metal d and NO π^* electrons.[8] Although this notation provides a general formalism, exact electronic descriptions of Fe−NO species are still the subjects of intense debate.[9−11] For example, a variety of descriptions of the electronic structures have been proposed for the $\{Fe-NO\}^7$ type of electron paramagnetic resonance (EPR) active NO-bound iron sites of non-heme iron enzymes[6] possessing either $S = {}^3/_2$ or $S = {}^1/_2$ ground states.[9] The synthetic $\{Fe-NO\}^7$ complexes with $S = {}^3/_2$,[12] $S = {}^1/_2$,[13] and $S = {}^3/_2-{}^1/_2$[14] ground states studied so far have not provided a consensus in this area. Very recently, a few diamagnetic $\{Fe-NO\}^6$ type of complexes have been studied in relation to the NO-bound (dark form) iron site of NHase.[15] Here also, an exact description of the electronic structure is yet to come. Thorough structural and spectroscopic studies on series of "isostructural" model complexes are clearly required for correct assignments of oxidation states of both iron and NO in all these Fe−NO species.

The Fe(III) site of NHase exhibits another interesting property of the $\{Fe-NO\}^6$ unit. Endo and co-workers have shown that binding of NO to the low-spin Fe(III) site in the dark converts the enzyme to an EPR-silent inactive form.[7] The iron-bound NO is lost upon illumination, a process that activates the enzyme toward hydrolysis of organic nitriles to amides. This regulation of the NHase activity by photolabile NO has inspired inorganic chemists to synthesize metal nitrosyls of the $\{Fe-NO\}^6$ type that exhibit photolability of bound NO since such nitrosyls could be used as light-induced NO donors in PDT. An exact electronic description of the $\{Fe-NO\}^6$ moiety in such nitrosyls will also provide insight into factors responsible for the observed photolability of bound NO in general.

We recently reported that a low-spin Fe(III) complex of the designed ligand $PaPy_3H$ ($PaPy_3H$ = *N*,*N*-bis(2-pyridylmethyl)amine-*N*-ethyl-2-pyridine-2-carboxamide), namely, $[(PaPy_3)Fe(MeCN)](ClO_4)_2$ (**1**), binds to a variety of ligands at the sixth site via replacement of the bound solvent molecule.[16] Complex **1** also binds NO very readily to afford a novel diamagnetic iron nitrosyl $[(PaPy_3)Fe(NO)](ClO_4)_2$ (**2**), which rapidly loses NO in acetonitrile upon illumination to visible light of low intensity (50-W tungsten lamp).[17] This photolability of NO observed with an iron nitrosyl of the $\{Fe-NO\}^6$ type closely resembles the behavior of the iron site in NHase. The extra stability provided to the +3 oxidation state of iron[18] appears to be related to the photolability of NO in the case of **2** since the Fe(III) and Fe(II) complexes of the Schiff base $SBPy_3$, a ligand identical to $PaPy_3H$ except for the presence of an imine group in place of the carboxamide moiety, do not show any reactivity toward either NO(g) or NO^+ under any condition.[19] We have

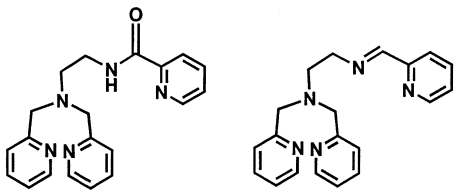

$PaPy_3H$ **$SBPy_3$**

now isolated and structurally characterized the one electron reduced product of **2**, namely, $[(PaPy_3)Fe(NO)](ClO_4)$ (**3**) (a nitrosyl of the $\{Fe-NO\}^7$ type). In this paper, we report the syntheses, structures, and spectral properties of $[(PaPy_3)Fe(NO)](ClO_4)_2$ (**2**) and $[(PaPy_3)Fe(NO)](ClO_4)$ (**3**). The electronic structures of the $\{Fe-NO\}^n$ unit in this set of

(5) (a) Ford, P. C.; Lorkovic, I. M. *Chem. Rev.* **2002**, *102*, 993. (b) Hoshino, M.; Laverman, L. E.; Ford, P. C. *Coord. Chem. Rev.* **1999**, *187*, 75. (c) Cooper, C. E. *Biochim. Biophys. Acta* **1999**, *1411*, 290.
(6) (a) Wolfe, M. D.; Parales, J. V.; Gibson, D. T.; Lipscomb, D. J. *J. Biol. Chem.* **2001**, *276*, 1945. (b) Orville, A. M.; Lipscomb, D. J. *J. Biol. Chem.* **1993**, *268*, 8596. (c) Chen, V. J.; Orville, A. M.; Harpel, M. R.; Frolik, C. A.; Surerus, K. K.; Münck, E.; Lipscomb, D. J. *J. Biol. Chem.* **1989**, *264*, 21677. (d) Nelson, M. J. *J. Biol. Chem.* **1987**, *262*, 12137. (e) Arciero, D. M.; Orville, A. M.; Lipscomb, D. J. *J. Biol. Chem.* **1985**, *260*, 14035. (f) Twilfer, H.; Bernhardt, F.-H.; Gersonde, K. *Eur. J. Biochem.* **1985**, *147*, 171.
(7) (a) Nagashima, S.; Nakasako, M.; Dohmae, N.; Tsujimura, M.; Takio, K.; Okada, M.; Yohda, M.; Kamiya, N.; Endo, I. *Nat. Struct. Biol.* **1998**, *5*, 347. (b) Odaka, M.; Fujii, K.; Hoshino, M.; Noguchi, T.; Tsujimura, M.; Nagashima, S.; Yohda, N.; Nagamune, T.; Inoue, I.; Endo, I. *J. Am. Chem. Soc.* **1997**, *119*, 3785.
(8) Enemerk, J. H.; Feltham, R. D. *Coord. Chem. Rev.* **1974**, *13*, 339.
(9) Brown, C. A.; Pavlosky, M. A.; Westre, T. E.; Zhang, Y.; Hedman, B.; Hodgson, K. O.; Solomon, E. I. *J. Am. Chem. Soc.* **1995**, *117*, 715.
(10) Franz, K. J.; Lippard, S. J. *J. Am. Chem. Soc.* **1999**, *121*, 10504.
(11) (a) Li, M.; Bonnet, D.; Bill, E.; Neese, F.; Weyhermuller, T.; Blum, N.; Sellmann, D.; Wieghardt, K. *Inorg. Chem.* **2002**, *41*, 3444. (b) Hauser, C.; Glaser, T.; Bill, E.; Weyhermuller, T.; Wieghardt, K. *J. Am. Chem. Soc.* **2000**, *122*, 4352.
(12) For selected references see: (a) Ray, M.; Golombek, A. P.; Hendrich, M. P.; Yap, G. P. A.; Liable-Sands, L. M.; Rheingold, A. L.; Borovik, A. S. *Inorg. Chem.* **1999**, *38*, 3110. (b) Westre, T. M.; Di Cicco, A.; Filiponi, A.; Natoli, C. R.; Hedman, B.; Solomon, E. I.; Hodgson, K. O. *J. Am. Chem. Soc.* **1994**, *116*, 6757. (c) Zhang, Y.; Pavlosky, M. A.; Brown, C. A.; Westre, T. E.; Hedman, B.; Hodgson, K. O.; Solomon, E. I. *J. Am. Chem. Soc.* **1992**, *114*, 9189. (d) Pohl, K.; Wiegardht, K.; Nuber, B.; Weiss, J. *J. Chem. Soc., Dalton Trans.* **1987**, 187.
(13) For selected references see: (a) Nasri, H.; Ellison, M. K.; Chen, S.; Huynh, B. H.; Scheidt, W. R. *J. Am. Chem. Soc.* **1997**, *119*, 6274. (b) Chen, Y.; Sweetland, A.; Shepherd, R. E. *Inorg. Chim. Acta* **1997**, *260*, 163. (c) Wayland, B. B.; Olson, L. W. *J. Am. Chem. Soc.* **1974**, *96*, 6037. (d) Goodman, B. A.; Raynor, J. B.; Symons, M. C. R. *J. Chem. Soc.* **1969**, 2572.
(14) (a) Wells, F. V.; McCann, S. W.; Wickman, H. H.; Kessel, S. L.; Hendrickson, D. N.; Feltham, R. D. *Inorg. Chem.* **1982**, *21*, 2306. (b) Haller, K. J.; Johnson, P. L.; Feltham, R. D.; Enemark, J. H. *Inorg. Chim. Acta* **1979**, *33*, 119. (c) Hodges, K. D.; Wollman, R. G.; Kessel, S. L.; Hendrickson, D. N.; Van Derveer, D. G.; Barefield, E. K. *J. Am. Chem.. Soc.* **1979**, *101*, 906.
(15) (a) Grapperhaus, C. A.; Patra, A. K.; Mashuta, M. S. *Inorg. Chem.* **2002**, *41*, 1039. (b) Chatel, S.; Chauvin, A. S.; Tuchagues, J. P.; Leduc, P.; Bill, E.; Chottard, J. C.; Mansuy, D.; Artaud, I. *Inorg. Chim. Acta* **2002**, *336*, 19. (c) Schweitzer, D.; Ellison, J. J.; Shoner, S. C.; Lovell, S.; Kovacs, J. A. *J. Am. Chem. Soc.* **1998**, *120*, 10996.
(16) Rowland, J. M.; Olmstead, M.; Mascharak, P. K. *Inorg. Chem.* **2001**, *40*, 2810.
(17) Patra, A. K.; Afshar, R.; Olmstead, M. M.; Mascharak, P. K. *Angew. Chem., Int. Ed.* **2002**, *41*, 2512.
(18) Marlin, D. S.; Mascharak, P. K. *Chem. Soc. Rev.* **2000**, *29*, 69.
(19) Patra, A. K.; Olmstead, M. M.; Mascharak, P. K. *Inorg. Chem.* **2002**, *41*, 5403.

structurally characterized $\{Fe-NO\}^6$ and $\{Fe-NO\}^7$ species have been established with the aid of structural and spectral parameters. A similar Fe(III) complex with an "innocent" NO_2^- ligand, namely, $[(PaPy_3)Fe(NO_2)](ClO_4)$ (**4**), is also reported. And finally, reactions of the coordinated NO in **2** and **3** with electrophiles such as O_2 and nucleophiles such as OH^- are described in detail.

Experimental Section

2-Aminomethylpyridine, *N*-bromoethylphthalimide, picolinic acid, and hydrazine monohydrate were purchased from Aldrich Chemical Co. and used without further purification. NO gas, procured from Johnson Mathew Chemical Co., was purified by passing through a KOH column. The starting metal salt, $[Fe(DMF)_6](ClO_4)_3$, and (2-aminoethyl)bis(2-pyridylmethyl)amine (DPEA) were synthesized by following published procedures.[20,21] All of the solvents were purified and/or dried by standard techniques and distilled prior to use. Standard Schlenk techniques were used during all syntheses to avoid exposure to dioxygen. Elemental analyses were performed by Atlantic Microlab Inc.

Synthesis Safety Note. Transition metal perchlorates should be handled with great caution and be prepared in small quantities as metal perchlorates are hazardous and may explode upon heating.

Syntheses of Compounds. The ligand *N*,*N*-bis(2-pyridylmethyl)-amine-*N*-ethyl-2-pyridine-2-carboxamide ($PaPy_3H$) was synthesized according to the literature procedure.[16]

$[(PaPy_3)Fe(NO)](ClO_4)_2$ (2). Method A. A slurry of 0.23 g of $[Fe(DMF)_6](ClO_4)_3$ (0.29 mmol) in 10 mL of MeOH was added to a stirred solution of $PaPy_3H$ (0.10 g, 0.29 mmol) in 10 mL of MeOH, followed by the addition of 1 equiv of NEt_3 (0.03 g, 0.3 mmol) dissolved in 2 mL of MeOH. The reaction mixture was then stirred at 45 °C for 30 min when a homogeneous reddish purple solution was obtained. Next, purified NO gas was allowed to pass through the solution for 1 min. The red-colored complex precipitated out immediately. It was then filtered, washed with anhydrous Et_2O, and dried under vacuum (0.095 g, 52% yield). Crystals of $[(PaPy_3)Fe(NO)](ClO_4)_2\cdot$MeCN (**2**·MeCN), suitable for X-ray diffraction, were grown via diffusion of Et_2O into a MeCN solution of the complex in the dark. Anal. Calcd for $C_{22}H_{23}Cl_2FeN_7O_{10}$ (**2**·MeCN): C, 39.31; H, 3.45; N, 14.59. Found: C, 39.28; H, 3.51; N, 14.60. Selected IR frequencies (KBr disk, cm^{-1}): 3082 (w), 2932 (w), 2867 (w), 1919 (vs), 1642 (vs), 1609 (m), 1453 (m), 1385 (m), 1289 (w), 1228 (w), 1090 (vs), 765 (m), 623 (m). Electronic absorption spectrum in MeCN (prepared in dark) λ_{max} (nm) (ϵ (M^{-1} cm^{-1})): 500 (1050), 365 (1850). ^1H NMR (500 MHz, CD_3CN, δ from TMS): 8.99 (d, 1H), 8.51 (t, 1H), 8.28 (d, 1H), 8.14 (t, 2H), 8.04 (m, 1H), 7.73 (d, 2H), 7.44 (t, 2H), 6.72 (d, 2H), 5.02 (dd, 4H), 3.73 (d, 2H), 3.68 (d, 2H).

Method B. A solution of 0.23 g of $[Fe(DMF)_6](ClO_4)_3$ (0.29 mmol) in 5 mL of MeCN was added to a stirred solution of $PaPy_3H$ (0.10 g, 0.29 mmol) in 7 mL of MeCN. Next, a solution of 1 equiv of NEt_3 (0.03 g, 0.3 mmol) in 5 mL of MeCN was added to the deep-purple solution. Passage of purified NO gas to this purple solution caused a sharp color change to red. The reaction mixture was further stirred for 1 h in dark and then subjected to Et_2O diffusion at 4 °C. After 2 days, the red crystals were filtered and washed with Et_2O and dried under vacuum (0.075 g, 41% yield).

$[(PaPy_3)Fe(NO)](ClO_4)$ (3). A solution of 0.122 g (0.35 mmol) of $PaPy_3H$ and 0.05 g (0.49 mmol) of NEt_3 in 20 mL of MeCN was thoroughly degassed by freeze−pump−thaw cycles. To the frozen MeCN solution of the ligand and base, a batch of solid $[Fe(MeCN)_4](ClO_4)_2$ (0.1 48 g, 0.35 mmol) was added and the frozen solution was allowed to warm to room temperature. The dark brownish red solution thus obtained was stirred for 30 min at room temperature. It was then cooled to 0 °C, and 11 mL (0.49 mmol) of NO was introduced to the reaction flask via a gastight syringe following evacuation. The resulting deep-brown reaction mixture was then stirred for 1 h. Next, a portion of 25 mL of Et_2O was added and the reaction mixture was stored at −20 °C for 12 h. The dark brown-red blocks were filtered and washed with small portions of Et_2O and dried (0.135 g, 62% yield). Anal. Calcd for $C_{24}H_{26}ClFeN_8O_6$ (**3**·2MeCN): C, 46.96; H, 4.23; N, 18.25. Found: C, 46.86; H, 4.19; N, 18.24. Selected IR frequencies (KBr disk, cm^{-1}): 3072 (w), 2942 (w), 2860 (w), 2284 (w), 2249 (m), 1613 (vs), 1590 (vs), 1454 (m), 1401 (w), 1373 (w), 1284 (m), 1219 (w), 1085 (vs), 761 (m), 620 (m). Electronic absorption spectrum in MeCN λ_{max} (nm) (ϵ (M^{-1} cm^{-1})): 830 (50), 476 (4300), 390 (sh, 3130), 370 (3170).

$[(PaPy_3)Fe(NO_2)](ClO_4)$ (4). Method A. A solution of 0.20 g (0.58 mmol) of $PaPy_3H$ in 15 mL of MeCN was added to a solution of 0.46 g (0.58 mmol) of $[Fe(DMF)_6](ClO_4)_3$ in 10 mL of MeCN. Next, a solution of 0.06 g (0.58 mmol) of NEt_3 in 7 mL of MeCN was slowly added to it with constant stirring. The deep-violet solution was stirred for 30 min, and then a batch of 0.125 g (1.81 mmol) of solid $NaNO_2$ was added to it. The color of the reaction mixture changed slowly to red after 3 h. It was then filtered to remove excess $NaNO_2$, and the volume of the filtrate was reduced to 15 mL. A portion of 15 mL of Et_2O was added, and the solution was stored at −20 °C for 24 h. The dark-red blocks were filtered and washed with Et_2O (0.32 g, 88% yield). Crystals of $[(PaPy_3)Fe(NO_2)](ClO_4)\cdot$2MeCN (**4**·2MeCN) were grown via diffusion of Et_2O into solution of the complex in MeCN at 4 °C. Anal. Calcd for $C_{24}H_{26}ClFeN_8O_7$ (**4**·2MeCN): C, 45.77; H, 4.13; N, 17.78. Found: C, 45.71; H, 4.09; N, 17.71. Selected IR frequencies (KBr disk, cm^{-1}): 3065 (w), 2958 (w), 2852 (w), 2249 (m), 1636 (vs), 1607 (vs), 1470 (m), 1446 (m), 1364 (s), 1280 (m), 1090 (vs), 764 (m), 622 (m). Electronic absorption spectrum in MeCN, λ_{max} (nm) (ϵ (M^{-1} cm^{-1})): 512 (2730), 390 (sh, 2190), 360 (sh, 3900), 340 (sh, 4125).

Method B. Conversion of 2 to 4. To a solution of 0.103 g (0.153 mmol) of **2** in 10 mL of MeCN was slowly added a dilute solution of NEt_4OH (0.102 g of a 40 wt % solution in water, 0.262 mmol) in 10 mL of MeCN in dark. The initial red color changed to red-purple, and the resulting reaction mixture was then stirred for 3 h. Next, it was concentrated to 5 mL and 5 mL of Et_2O was added to it. Storage of this mixture at −20 °C for 12 h afforded 0.085 g of **4** as dark-red blocks (89% yield).

Method C. Conversion of 3 to 4. A batch of 0.045 g (0.073 mmol) of solid **3** was added to 5 mL of MeCN that had been thoroughly degassed by freeze−pump−thaw cycles. The brown-red solution was then exposed to dioxygen, and the color changed immediately to purple-red. The reaction mixture was stirred for 2 h and then stored at −20 °C following addition of 7 mL of dry Et_2O. Deep-red crystals of **4** were formed within 4 h. The crystals were filtered and washed with dry Et_2O (0.04 g, 86% yield).

Physical Methods. Absorption spectra were recorded on a Cary 50 Varian spectrophotometer. A Perkin-Elmer 1600 FTIR spectrophotometer was employed to monitor the infrared spectra. ^1H NMR spectra were recorded at 25 °C on a Bruker 500 MHz spectrometer. X-Band EPR spectra were obtained in MeCN glass (~0.01 mM with excess $[^tBu_4N][PF_6]$ added to help prevent intermolecular interactions) with a Bruker ELEXSYS E300 spec-

(20) Hodgkinson, J.; Jordan, R. B. *J. Am. Chem. Soc.* **1973**, *95*, 763.
(21) Matouzenko, G. S.; Bousseksou, A.; Lecocq, S.; van Koningsbruggen, P. J.; Perrin, M.; Kahn, O.; Collet, A. *Inorg. Chem.* **1997**, *36*, 2975.

Table 1. Summary of Crystal Data, Intensity Collection, and Structural Refinement Parameters for $[(PaPy_3)Fe(NO)](ClO_4)_2$·MeCN (**2**·MeCN), $[(PaPy_3)Fe(NO)](ClO_4)$·2MeCN (**3**·2MeCN), and $[(PaPy_3)Fe(NO_2)](ClO_4)$·2MeCN (**4**·2MeCN)

	2	**3**	**4**
formula	$C_{22}H_{23}Cl_2FeN_7O_{10}$	$C_{24}H_{26}ClFeN_8O_6$	$C_{24}H_{26}ClFeN_8O_7$
mol wt	672.22	613.83	629.83
cryst color, habit	red plate	red block	red block
T, K	91(2)	90(2)	90(2)
cryst syst	orthorhombic	monoclinic	monoclinic
space group	*Pbca*	$P2_1$	$P2_1/n$
a, Å	7.740(3)	8.2530(4)	13.1985(4)
b, Å	21.990(9)	13.9435(7)	14.1008(5)
c, Å	30.634(11)	11.7823(6)	15.3473(5)
α, deg	90	90	90
β, deg	90	99.225(3)	105.5280(10)
γ, deg	90	90	90
V, Å^3	5214(3)	1338.32(12)	2752.02(16)
Z	8	2	4
d_{calcd}, g cm^{-3}	1.713	1.523	1.520
abs coeff, mm^{-1}	0.855	0.719	0.704
GOF[a] on F^2	1.059	1.017	0.908
R1,[b] %	4.76	3.09	3.91
Rw2,[c] %	11.86	6.87	9.07

[a] GOF = $[\sum w(F_o^2 - F_c^2)^2]/(M - N)^{1/2}$ (M = number of reflections, N = number of parameters refined). [b] R1 = $\sum||F_o| - |F_c||/\sum|F_o|$. [c] Rw2 = $[[\sum w(F_o^2 - F_c^2)^2]/\sum w(F_o)^2]^{1/2}$.

trometer with standard cavity and Oxford Instruments ESR910 flow cryostat. Spin-Hamiltonian simulations were performed with the XSOPHE program by G. Hanson et al. that is distributed by Bruker Biospin GmbH. Magnetization of solid **3** was measured using a SQUID magnetometer (MPMS-7, Quantum Design). The molar susceptibilities were corrected for underlying diamagnetism using tabulated Pascal constants ($\chi_{dia} = -300 \times 10^{-6}$ cm^3 mol^{-1}).[22] The routine JULIUS was used for spin-Hamiltonian simulation.[23] Mössbauer spectra were recorded with a conventional Mössbauer spectrometer operating in a constant acceleration mode and equipped with a ^{57}Co/Rh source at room temperature. The spectra were analyzed by a least-squares fit procedure using Lorentzian line shape. All isomer shift (δ) and quadrupole splitting (ΔE_Q) values are reported with respect to ^{57}Fe-enriched metallic iron foil that was used for velocity calibration. Changes in the electronic absorption spectra due to loss of NO from **2** upon illumination were recorded as follows. The cuvette containing a 0.4 mM solution of **2** in MeCN was placed 5 cm away from a 50-W tungsten lamp for 30-s intervals, and the absorption spectra were monitored on a Cary 50 spectrophotometer in fast scan mode (spectra shown in Figure 10).

Photolysis Experiments. Kinetic studies on the photolysis reactions were carried out with a Cary 50 Varian spectrophotometer. A Varian fiber optics probe was employed to detect the absorbance values at fixed wavelengths. The tip of the probe was placed inside a 5 dram capped vial containing ~0.4×10^{-3} M solution of **2** (prepared in dark). Three different solvents (MeCN, DMF, and H_2O) were used. The vial was held at a fixed distance of 5 cm from the light source. Tungsten lamps of different power (25, 60, and 100 W) were used as the light source. Periodic scanning of the absorbance values at 550 nm was carried out in the case of MeCN solution, whereas in the cases of DMF and H_2O, the wavelength was held fixed at 510 nm. These wavelengths were chosen to achieve the maximum changes in the absorption spectra. Data collection began as the light was turned on. Observed rate constant values K_{NO} were evaluated by fitting the kinetic traces to the equation $A(t) = A_\infty + (A_0 - A_\infty)\{\exp(-K_{NO}t)\}$, where A_0 and A_∞ are the initial and final absorbance values at the fixed wavelength, respectively. The rate constants shown in Table 5 are the mean values of three independent measurements in each case.

X-ray Data Collection and Structure Solution and Refinement. Diffraction data for **2**−**4** were collected at 90 K on a Bruker SMART 1000 system. Mo Kα (0.71073 Å) radiation was used, and the data were corrected for absorption. The structures were solved by direct methods (standard SHELXS-97 package). In **4**, the oxygen atoms of the nitro group are disordered. This disorder problem had been tackled by refinement with fractional occupancy of two sets of oxygen atoms. The best meaningful refinement was obtained with 0.752(5) occupancy for the set O2A/O3A and 0.248(5) occupancy for the set O2B/O3B. All non-hydrogen atoms were refined with anisotropic displacement parameters, and hydrogen atoms were added geometrically and refined with the use of a riding model. Machine parameters, crystal data, and data collection parameters for all the complexes are summarized in Table 1 while selected bond distances and angles are listed in Table 2. Complete crystallographic data for $[(PaPy_3)Fe(NO)](ClO_4)_2$·MeCN (**2**·MeCN), $[(PaPy_3)Fe(NO)](ClO_4)$·2MeCN (**3**·2MeCN), and $[(PaPy_3)Fe(NO_2)](ClO_4)$·2MeCN (**4**·2MeCN) have been submitted as Supporting Information.

Results and Discussion

Syntheses and Interconversions. The pentadentate ligand $PaPy_3H$ has been synthesized in high yield by condensation of (2-aminomethyl)bis(2-pyridylethyl)amine (DPEA) and 2-picolyl chloride in the presence of NEt_3 as the base. This ligand with one carboxamide group has been reported by us in a previous paper.[16] Although we have utilized NaH to deprotonate the carboxamide group of $PaPy_3H$ before, results of the present work show that a mild base is sufficient for such deprotonation in the presence of a metal ion. Thus the complex $[(PaPy_3)Fe(MeCN)](ClO_4)_2$ (**1**) can be generated by the addition of $[Fe^{III}(DMF)_6](ClO_4)_3$ to a mixture of $PaPy_3H$ and NEt_3 (1:1) in MeCN. When purified NO(g) is passed through a solution of **1** in MeCN, the purple solution rapidly turns red, showing the formation of the NO adduct $[(PaPy_3)Fe(NO)](ClO_4)_2$ (**2**). However, the photolability of the bound NO in **2** under light does not allow one to synthesize **2** in

(22) Earnshaw, A. *Introduction to Magnetochemistry*; Academic Press: New York, 1968.
(23) Krebs, C.; Bill, E.; Birkelbach, F.; Staemmler, V. unpublished.

Scheme 1

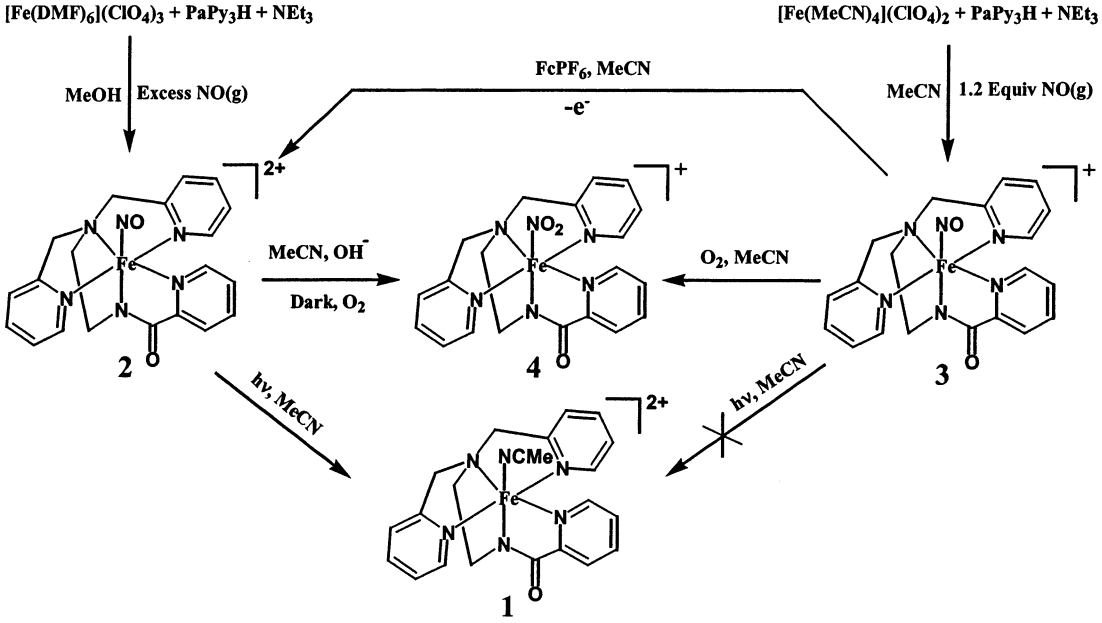

Table 2. Selected Bond Distances [Å] and Bond Angles [deg]

	complex **2**	complex **3**	complex **4**
Fe−N1	1.978(2)	1.9801(15)	1.9856(14)
Fe−N2	1.9009(19)	1.9577(15)	1.8563(13)
Fe−N3	1.972(2)	1.9946(16)	1.9847(14)
Fe−N4	1.982(2)	1.9836(15)	1.9648(15)
Fe−N5	1.983(2)	1.9990(15)	1.9637(14)
Fe−N6	1.677(2)	1.7515(16)	2.0436(15)
N6−O2/O(2A)	1.139(3)	1.190(2)	1.235(2)
N6−O(3A)			1.195(2)
N6−O(2B)			1.245(7)
N6−O(3B)			1.169(8)
C6−O1	1.233(3)	1.247(2)	1.2327(19)
C6−N2	1.341(3)	1.322(2)	1.342(2)
N1−Fe−N2	81.18(8)	80.07(6)	83.05(6)
N1−Fe−N3	165.68(8)	164.15(6)	168.77(6)
N1−Fe−N4	97.13(9)	95.44(6)	97.15(6)
N1−Fe−N5	95.88(8)	98.14(6)	96.31(6)
N1−Fe−N6	96.78(9)	96.84(7)	94.55(6)
N2−Fe−N3	84.58(8)	84.29(6)	85.78(6)
N2−Fe−N4	91.82(8)	91.38(6)	96.21(6)
N2−Fe−N5	84.35(8)	86.08(6)	88.13(6)
N2−Fe−N6	174.35(9)	176.91(7)	175.18(6)
N3−Fe−N4	81.79(9)	82.33(6)	82.80(6)
N3−Fe−N5	84.13(8)	83.25(6)	84.53(6)
N3−Fe−N6	97.54(9)	98.80(7)	96.68(6)
N4−Fe−N5	165.71(8)	165.53(6)	166.26(6)
N4−Fe−N6	93.67(9)	88.92(7)	88.23(6)
N5−Fe−N6	90.64(9)	94.38(7)	87.98(6)
Fe−N6−O2/O2A	173.1(2)	141.29(15)	116.00(14)
Fe−N6−O3A			120.77(13)
Fe−N6−O2B			116.6(3)
Fe−N6−O3B			121.0(4)

pure form by this route. In our modified method, a slurry of $[Fe^{III}(DMF)_6](ClO_4)_3$ and $PaPy_3H$ (1:1) in methanol is first stirred with 1 equiv of a mild base such as NEt_3 at 45 °C. The mixture became homogeneous and reddish purple within 30 min. Passage of NO through this solution causes rapid precipitation of red microcrystalline **2** in pure form and in good yield. The absence of photolability of bound NO in the case of Fe(II) species however allows one to synthesize $[(PaPy_3)Fe(NO)](ClO_4)$ (**3**) by the reaction of 1 equiv of NO gas with a solution of $PaPy_3H$, NEt_3, and $[Fe(MeCN)_4](ClO_4)_2$ in MeCN under strictly anaerobic conditions. Complex **3** is readily converted into **2** by oxidation with ferrocinium salts in MeCN. Complex **3** is also quite sensitive to dioxygen, and exposure of a solution of **3** to dioxygen affords the nitro complex $[(PaPy_3)Fe(NO_2)](ClO_4)$ (**4**) in quantitative yield. The nitro complex **4** can be independently synthesized by the reaction of $NaNO_2$ and **1** in MeCN. The electrophilic nature of the bound NO in **2** (vide infra) also allows one to synthesize **4** from **2** by the addition of a stoichiometric amount of OH^- under aerobic conditions. These results are summarized in Scheme 1.

Structures of the Complexes. $[(PaPy_3)Fe(NO)](ClO_4)_2$·MeCN (2·MeCN). The structure of $[(PaPy_3)Fe(NO)]^{2+}$ (the cation of **1**) is shown in Figure 1, and selected bond distances and angles are listed in Table 2. The pentadentate monoanionic ligand $PaPy_3^-$ is bound to the Fe(III) center in a fashion such that the three pyridine nitrogens and the tertiary nitrogen reside in the equatorial plane while the carboxamido nitrogen occupies a position trans to the bound NO. This

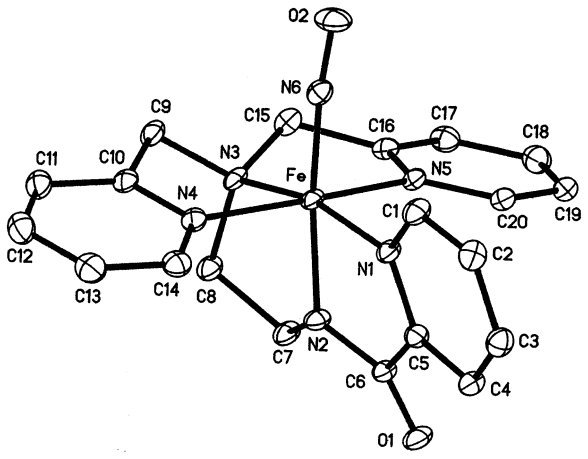

Figure 1. Thermal ellipsoid (probability level 50%) plot of $[(PaPy_3)Fe(NO)]^{2+}$ (cation of **2**) with the atom-labeling scheme. H atoms are omitted for the sake of clarity.

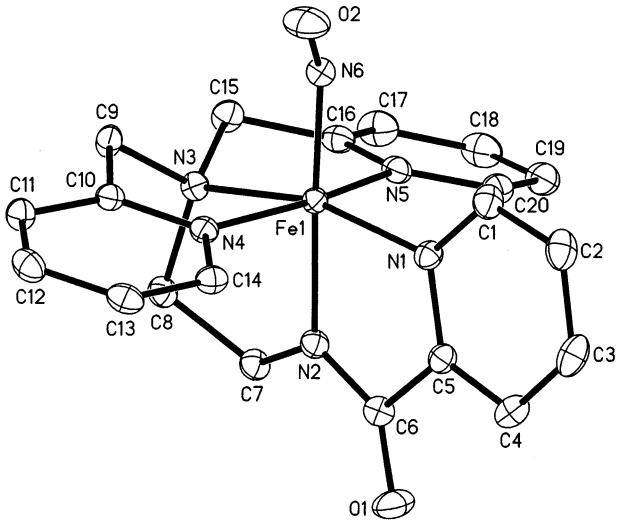

Figure 2. Thermal ellipsoid (probability level 50%) plot of $[(PaPy_3)Fe(NO)]^+$ (cation of **3**) with the atom-labeling scheme. H atoms are omitted for the sake of clarity.

mode of coordination of $PaPy_3^-$ to the Fe(III) center has been observed before in **1** and related complexes.[16] In all such $[(PaPy_3)Fe(X)]^{n+}$ complexes, the carboxamido nitrogen occupies an axial position trans to X.

The Fe−N(O) bond distance (1.677(2) Å) of **2** lies in the range of such distances in other structurally characterized $\{Fe-NO\}^6$ complexes (1.6−1.7 Å)[15,24a] and is quite comparable to the Fe−N(O) distance of the dark form of the enzyme (1.65 Å).[7a] Both the short Fe−N(O) distance, evidence of appreciable double bond character, and an almost linear Fe−N−O angle (173.1(2)°) of **2** are typical of $\{Fe-NO\}^6$ nitrosyls.[15] The average $Fe-N_{py}$ (1.981(2) Å) and $Fe-N_{amine}$ (1.972(2) Å) distances of **2** are very similar to those noted for **1** ($Fe-N_{py}$ = 1.970(3) Å and $Fe-N_{amine}$ = 1.972(3) Å) while the $Fe-N_{amido}$ distance (1.9009(19) Å) is noticeably longer than that in **1** (1.826(3) Å).[16] This lengthening is presumably due to the trans influence of the sixth ligand (NO in **2** vs MeCN in **1**). It is interesting to note that the $Fe-N_{amido}$ distance (1.9009(19) Å) of **2** is comparable to the average $Fe-N_{amido}$ distance (1.925(8) Å) of the Fe(III) complex of (2-mercapto-isobutyryl)-*o*-phenylenediamine, the only other $\{Fe-NO\}^6$ type iron nitrosyl with carboxamido nitrogen and thiolato sulfur donors.[15b]

$[(PaPy_3)Fe(NO)](ClO_4)\cdot 2MeCN$ (3·2MeCN). The structure of $[(PaPy_3)Fe(NO)]^+$, the cation of complex **3**, is shown in Figure 2, and selected bond distances and angles are included in Table 2. Although the distorted octahedral geometry around iron in this $\{Fe-NO\}^7$ iron nitrosyl is similar to that observed in **2**, appreciable differences in metric parameters are noted along the $N_{amido}-Fe-N-O$ vector. For example, the Fe−N(O) bond length of **3** is 0.074 Å longer than that of **2**, and the Fe−N−O angle is significantly smaller (141.29(15)°). Both the Fe−N(O) distance and the smaller Fe−N−O angle of **3** are typical of $\{Fe-NO\}^7$ type of iron nitrosyls.[11b,12a,24,25] The N−O distance of **3** (1.190(2) Å) is close to the N−O distance of free NO (1.15 Å) but far from the N−O distance of NO^- (1.26 Å).

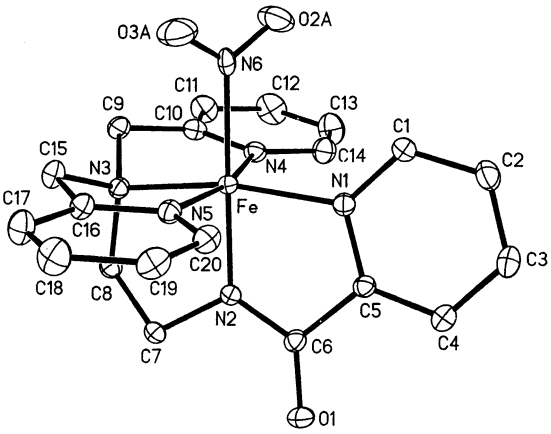

Figure 3. Thermal ellipsoid (probability level 50%) plot of $[(PaPy_3)Fe(NO_2)]^+$ (cation of **4**) with the atom-labeling scheme. H atoms are omitted for the sake of clarity.

Table 3. Selected Bond Distances in Iron Complexes of $PaPy_3H$

complex	N2−C6 (Å)	C6−O1 (Å)	Fe−N2 (Å)	ref
$[Fe(PaPy_3)(MeCN)]^{2+}$	1.349(4)	1.237(4)	1.826(3)	16
$[Fe(PaPy_3)(Cl)]^+$	1.340(3)	1.233(3)	1.8559(17)	16
$[Fe(PaPy_3)(CN)]^+$	1.342(3)	1.238(3)	1.858(2)	16
$[Fe(PaPy_3)(NO)]^{2+}$	1.341(3)	1.233(3)	1.9009(19)	*a*
$[Fe(PaPy_3)(NO)]^+$	1.322(2)	1.247(2)	1.9577(15)	*a*
$[Fe(PaPy_3)(NO_2)]^+$	1.342(2)	1.2327(19)	1.8563(13)	*a*

[a] This work.

$[(PaPy_3)Fe(NO_2)](ClO_4)\cdot 2MeCN$ (4·2MeCN). The structure of $[(PaPy_3)Fe(NO_2)]^+$, the cation of **4**, is shown in Figure 3, and selected bond distances and angles are listed in Table 2. In this complex, the geometry around the Fe(III) center is distorted octahedral and the $PaPy_3^-$ ligand is coordinated in the same fashion. The $Fe-N_{amido}$ bond is 1.8563(13) Å long. This value is very close to the $Fe-N_{amido}$ distances of $[(PaPy_3)Fe(X)]^+$ ($X = Cl^-, CN^-$)[16] but is noticeably smaller than those of **2** and **3** (Table 3). The average metric parameters of the bound nitro group matches well with those observed in $[L(NO)(ONO)(NO_2)]^+$ (where L is 1,4,7-triazacyclononane)[11b] and $[Fe(NO)(NO_2)(S_2CN(C_2H_5)_2)_2]$.[26]

Comparison of Structural Parameters. A close scrutiny of the structures of **2**−**4** (Figures 1−3, Table 2) reveals that the metric parameters of the equatorial plane of these three complexes are very similar to one another. However, significant differences exist along the $N_{amido}-Fe-N-O$ vector (axial) in these three complexes. The metric parameters of the axial coordination are shown in Figure 4. Comparison of the $\{Fe-NO\}^6$ and the $\{Fe-NO\}^7$ species (**2** and **3**, respectively) clearly indicates that both the Fe−N and N−O distances increase upon addition of one electron (structure B). The almost linear Fe−N−O angle in **2** (structure A) and shorter Fe−N and N−O distances support partial transfer of electron density from the NO ligand to the formal Fe(III) center. The situation changes significantly

(24) (a) Sellmann, D.; Blum, N.; Heinemann, F. W.; Hess, B. A. *Chem.−Eur. J.* **2001**, 7, 1874. (b) Sellman, D.; Kunstmann, H.; Moll, M.; Knoch, F. *Inorg. Chim. Acta* **1988**, *154*, 157.

(25) (a) Scheidt, W. R.; Frisse, M. E. *J. Am. Chem. Soc*. **1975**, *97*, 17. (b) Berno, P.; Floriani, C.; Chiesi-Villa, A.; Guastini, C. *J. Chem. Soc., Dalton Trans.* **1988**, 1409.

(26) Ileperuma, O. A.; Feltham, R. D. *Inorg. Chem.* **1977**, *16*, 1876.

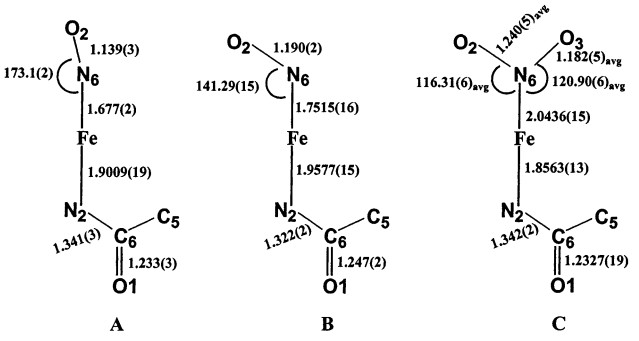

Figure 4. Metric parameters of the axial coordination in **2**−**4**.

when NO is bonded to the formal Fe(II) center in **3**. Here, the Fe−N−O angle is much smaller and the N−O bond is longer. These facts imply that the single electron in the antibonding orbital of NO is more localized on itself in **3**. It is also interesting to note the change in the Fe−N_{amido} distance as one goes from **3** to **2**. This distance decreases noticeably as the iron center approaches the +3 oxidation state. In the case of **4**, a true Fe(III) complex, the Fe−N_{amido} distance is even smaller, indicating the clear preference of Fe(III) center for carboxamido N.[18]

Another interesting difference is observed in the coordinated carboxamido moiety in the {Fe−NO}^{7} complex **3**. The C−O bond length of the carbonyl portion is 0.01 Å longer than all other structurally characterized Fe(III) complexes (Table 3). Also, the N2−C6 distance in **3** is shorter than all other Fe(III) complexes derived from $PaPy_3^-$ (Table 3). Collectively, these two differences imply a partial single bond character in the carbonyl moiety (normal C−O distance ∼ 1.43 Å, normal C=O distance is ∼1.20 Å) in **3**.[27] In complexes with deprotonated amide group coordinated to the metal center through the N atom, delocalization of the negative charge on the N atom over the amide N−C(=O) moiety gives rise to two resonance forms (**a** and **b**) which have different C−N and C−O bond orders. In resonance

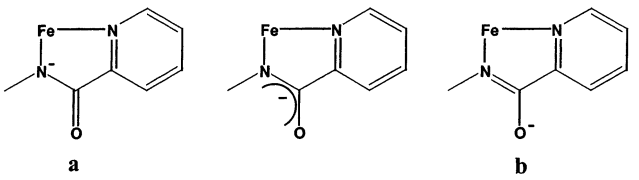

form **a**, the C−O portion has more double bond character and the Fe−N_{amido} bond length is relatively short. Resonance form **b** on the other hand, comprises a C−N portion with more double bond character and the Fe−N_{amido} bond is longer. The bond distances in Table 3 indicate that genuine Fe(III) complexes such as $[Fe(PaPy_3)(Cl)]^+$ and $[Fe(PaPy_3)(NO_2)]^+$ (**4**) are better represented by the resonance form **a** while in the case of **3**, resonance form **b** has a significant contribution.

Spectroscopic Properties. Complex **2** displays a strong NO stretch (ν_{NO}) at 1919 cm^{-1}, which is in the range (1822−1937 cm^{-1}) expected for an {Fe−NO}^{6} type complex.[15] The ^{1}H NMR spectrum of this complex (prepared and run in the dark) clearly indicates its $S = 0$ ground state (Figure 5). Quite in contrary, the ν_{NO} of **3** (a {Fe−NO}^{7} type complex) is red shifted and merges with ν_{CO} at ∼1615 cm^{-1} (broad strong band). Similar shift in ν_{NO} has been reported in other {Fe−NO}^{7}-type iron nitrosyls.[11b,24] In all three complexes (**2**−**4**), coordination of deprotonated carboxamido N to the iron center is indicated by red shift of ν_{CO} (1613−1642 cm^{-1} compared to 1666 cm^{-1} for free ligand).

The absorption spectra of **2**−**4** in MeCN are displayed in Figure 6. All three complexes display two strong absorption maxima at ∼500 and ∼350 nm, which are of LMCT origin. Similar bands have been noted previously in other iron complexes derived from $PaPy_3H$.[16] Interestingly, both the positions and the relative intensity of these two bands change significantly in $[Fe(PaPy_3)(X)]^{n+}$ complexes depending on the sixth ligand X. For example, in the case of complexes with X = Cl^-, CN^-, NO_2^-, and linear NO, the ∼350 nm band is more intense than the ∼500 nm band. Quite in contrary, for complexes with X = N_3^-, MeCN, and bent NO group, the ∼500 nm band is more intense than the band at ∼350 nm. This fact allows one to readily distinguish between the {Fe−NO}^{6} (**2**) and {Fe−NO}^{7} (**3**) species in the present case. In addition to these two bands, **3** also shows a broad and weak (ϵ = 50 M^{-1} cm^{-1}) absorption with maximum at 830 nm. This weak absorption arises from d−d transition. Similar absorption has been observed for other non-heme {Fe−NO}^{7} complexes.[12a,28]

Complex **3** is paramagnetic and displays EPR signal at $g \sim 2$, suggesting an $S = {}^1/_2$ ground state. The X-band EPR spectrum of **3** in dilute acetonitrile glass (20 K) is shown in Figure 7 (top panel). A rhombic $S = {}^1/_2$ signal is observed at $g_x = 2.026$, $g_y = 2.004$, and $g_z = 1.938$ with a distinct hyperfine splitting at g_y (for g_x and g_z, the hyperfine pattern is not resolved). The spectrum is reasonably well simulated by including hyperfine splitting from *one* nitrogen ligand with parameters $A_x(^{14}N) = 14 \times 10^{-4}$ cm^{-1} (42 MHz), $A_y(^{14}N) = 24 \times 10^{-4}$ cm^{-1} (72 MHz), and $A_z(^{14}N) = 11 \times 10^{-4}$ cm^{-1} (33 MHz). Only A_y can be uniquely determined while A_x and A_z are estimates that are derived from the widths of the respective powder lines. Wieghardt and co-workers have demonstrated that in {Fe−NO}^{7} complexes, significant delocalization occurs in the Fe−NO bond.[11a] We believe that in **3**, the ^{14}N hyperfine splitting of the NO ligand is also dominating over that of other N donors of the $PaPy_3^-$ ligand. The strength of the N coupling, which corresponds to the spin density at the ^{14}N nucleus of NO, compares well with what was observed previously for other non-heme nitrosyl complexes with $S = {}^1/_2$ ground state.[11]

The electronic g values of **3** are remarkably close to g = 2.002, the free electron value, in contrast to those of the genuine low-spin Fe(III) complexes with the same ligand. For example, the g values for $[Fe(PaPy_3)(Cl)]^+$ are 2.450, 2.219, and 1.875 while those for **4** are 2.347, 2.212, and 1.902. The large g anisotropy of the latter set of complexes

(27) (a) McLachlan, G. A.; Brudenell, S. J.; Fallon, G. D.; Martin, R. L.; Spiccia, L.; Tiekink, E. R. T. *J. Chem. Soc., Dalton Trans.* **1995**, 439. (b)Machida, R.; Kimura, E.; Kushi, Y. *Inorg. Chem.* **1986**, *25*, 3461.

(28) Chiou, Y.-M.; Que, L., Jr. *Inorg. Chem.* **1995**, *34*, 3270.

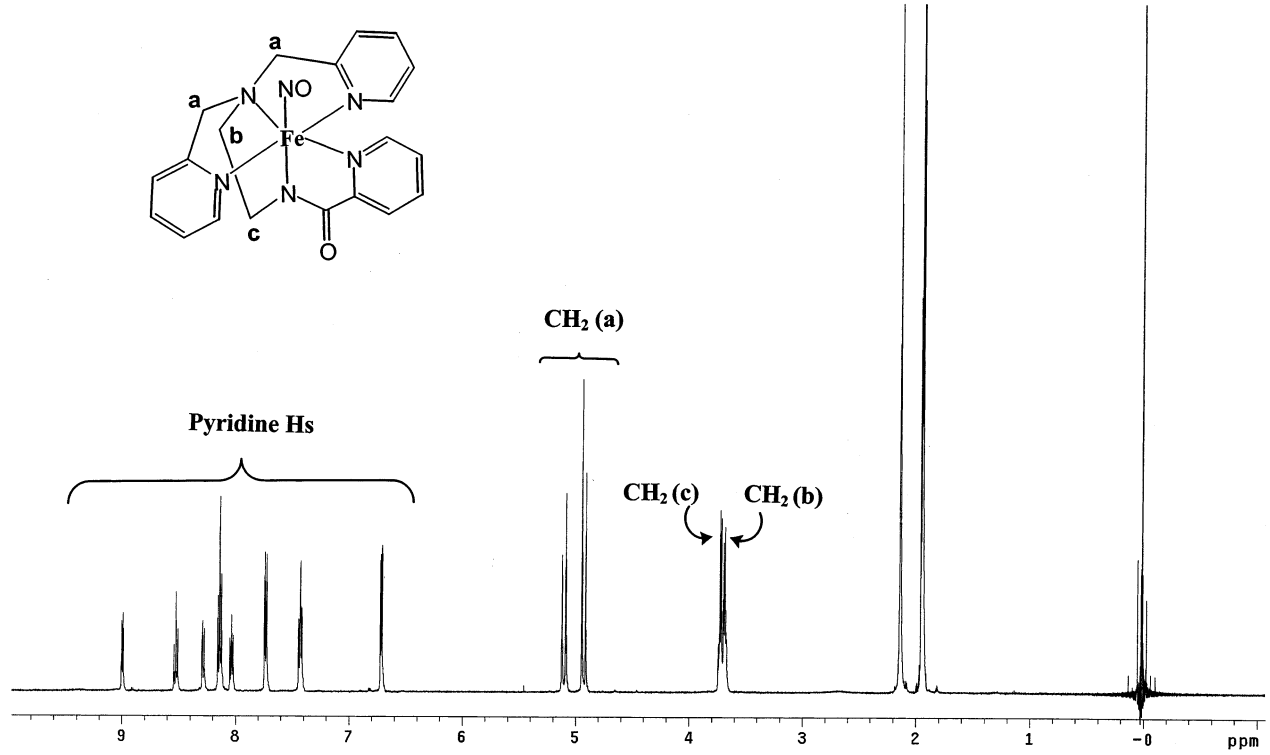

Figure 5. ^{1}H NMR spectrum (500 MHz) of $[(PaPy_3)Fe(NO)](ClO_4)_2$ (**2**) in CD_3CN (295 K).

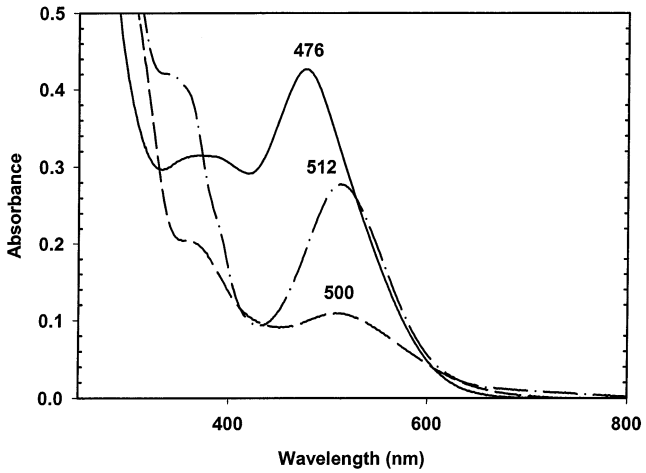

Figure 6. Electronic absorption spectra of 0.1 mM solutions of **2** (broken line), **3** (solid line), and **4** (dash−dot line) in MeCN.

with "innocent" sixth ligands is typical of $(t_{2g})^5$ configuration of low-spin Fe(III) due to strong spin−orbit interaction of the "hole" in the t_{2g} subshell.[29] It is therefore evident that the iron center in **3** is best described as low-spin Fe(II) ($(t_{2g})^6$) with coordinated NO•. This is also supported by the longer Fe−N(O) and N−O distances as well as the bent NO group in **3** (Figure 4).

The $S = {}^1/_2$ ground state of **3** has also been established by variable-temperature susceptibility measurements performed with a SQUID magnetometer. The temperature dependence of effective magnetic moment of **3** in an external magnetic field of 1 T is shown in the bottom panel of Figure 7. The fit shown in Figure 7 has been obtained by using the following parameters, a fixed $g = 2.01$ and a temperature-independent paramagnetism, χ_{TIP}, of 0.23×10^{-3} cm^3 mol^{-1}.

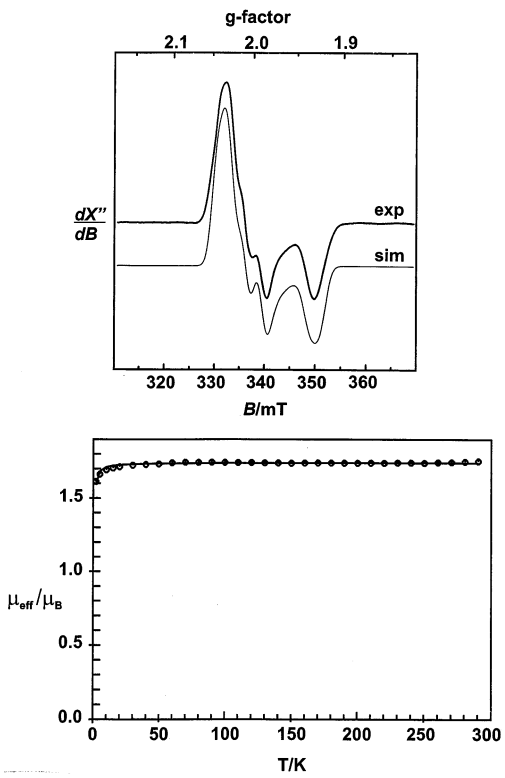

Figure 7. (Top) X-band EPR spectrum of **3** in MeCN glass at 20 K. Instrument settings: microwave frequency, 9.45 GHz; power, 2 μW; modulation (100 kHz), 0.8 mT. The simulated spectrum was obtained with $g = 2.026$, 2.004, and 1.938, with A_N ($x = -14$, $y = -24$, $z = -10.5$) $\times$ 10^{-4} cm^{-1}, and with Gaussian line width $W = 10 \times 10^{-4}$ cm^{-1}. (Bottom) Temperature dependence of magnetic moment μ_{eff}/μ_B of a solid sample of **3**. The solid line represents best fit using the parameters given in the text.

(29) Oosterhuis, W. T.; Lang, G. *Phys. Rev.* **1969**, *178*, 439.

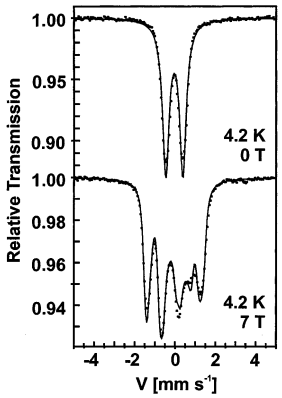

Figure 8. (Top) Zero-field Mössbauer spectrum of solid **2** at 4.2 K. (Bottom) Applied-field (7 T) Mössbauer spectrum of solid **2** at 4.2 K.

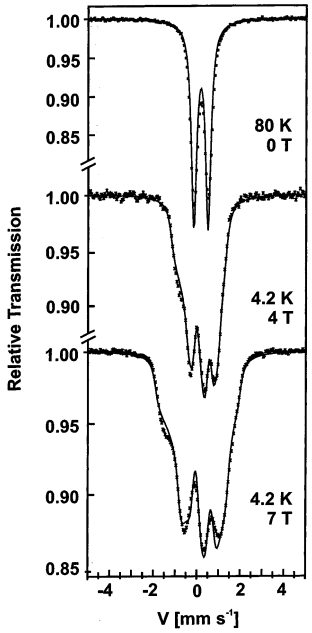

Figure 9. (Top) Zero-field Mössbauer spectrum of solid **3** at 80 K. (Bottom) Applied-field Mössbauer spectra of solid **3** at 4.2 K.

The susceptibility value clearly indicates that this $\{Fe-NO\}^7$ species has a $S = {}^1/_2$ ground state much like *trans*-[(cyclam)-Fe(NO)(Cl)](ClO_4).[11b]

The zero-field Mössbauer spectra of **2** and **3** recorded at 4.2 and 80 K, respectively, are shown in the top panels of Figures 8 and 9, respectively. The spectra consist of quadrupole doublets with isomer shifts $\delta = -0.05$ and 0.18 mm s^{-1}, and quadrupole splittings, $\Delta_{eq} = +0.85$ and $+0.66$ mm s^{-1}, respectively. The sign of *Vzz*, the main component of the electric field gradient tensor (efg), and the asymmetry parameter η_0 of the efg were obtained from the magnetically perturbed Mössbauer spectra described below. The isomer shift differs substantially between the $\{Fe-NO\}^6$ (**2**) and $\{Fe-NO\}^7$ (**3**) complexes. However, even more significant is the difference in quadrupole splittings between the nitrosyls (**2** and **3**) on one hand and the Fe(III) complexes with "innocent" sixth ligands (like $[Fe(PaPy_3)(Cl)]^+$ and **4**) on the other. The latter complexes exhibit very large negative quadrupole splittings (-2.67 and -2.65 mm s^{-1} for $[Fe(PaPy_3)(Cl)]^+$ and **4**, respectively) with values typical of low-spin Fe(III). These high values arise from strong valence contributions to the efg, originating from the "hole" in the t_{2g} set of iron d-orbitals. This is in accordance with the EPR results mentioned above. In contrast, the low quadrupole splittings of **2** and **3** indicate vanishing valence contributions to the efg and, hence, a different electronic configuration should prevail in these two iron nitrosyls.

Table 4. Spin-Hamiltonian and Hyperfine Parameters of Complexes **2**−**4** and $[(PaPy_3)Fe(Cl)](ClO_4)$ Obtained at Liquid He Temperature

	2	**3**	**4**	$[(PaPy_3)Fe(Cl)]^+$
S	0	$^1/_2$	$^1/_2$	$^1/_2$
δ, mm s^{-1}	−0.05	0.18	0.19	0.21
ΔE_Q, mm s^{-1}	+0.85	+0.66	−2.65	−2.67
η	0.5	<0.1	<0.1	0.2
g_x		2.026	2.347	2.450
g_y		2.004	2.212	2.219
g_z		1.938	1.902	1.875
$A_x/g_N\beta_N$, T		−17.21	−46.51	−31.60
$A_y/g_N\beta_N$, T		−6.01	−15.87	−56.50
$A_z/g_N\beta_N$, T		+12.02	−39.86	+4.10
$A_{iso}/g_N\beta_N$, T		−3.73	−34.08	−28.00

To determine the strength of the internal fields (a measure of spin density) at the iron nuclei of **2** and **3**, magnetic Mössbauer spectra of both complexes were recorded on powder samples at liquid He temperature under different applied magnetic fields. The spectra are shown in the bottom panels of Figures 8 and 9, respectively. The magnetic hyperfine pattern of **2** can be readily simulated without any internal field, a fact that attests its $S = 0$ spin state, as expected for a $\{Fe-NO\}^6$ system. The magnetic spectra of the $\{Fe-NO\}^7$ species, however, clearly disclose spin density at the iron nucleus and anisotropic hyperfine coupling interaction with significant spin-dipolar contributions that are described by an anisotropic hyperfine coupling tensor listed in Table 4. We note that the main component of the efg tensor, listed in Table 4, is oriented virtually along the *x*-component of the **A**-tensor (12° misalignment, Euler angle for the efg = 102°). The isotropic part of the **A**-tensor is strikingly low ($A_{iso}/g_N\mu_N = {}^1/_3$ tr(A) = −3.7 T) for **3**. It is far from $A_{iso}/g_N\mu_N = -16$ to -20 T as would be typically expected for a fully iron-centered spin $S = {}^1/_2$. Apparently, the Fermi contact contribution to the **A**-tensor that is determined by the spin density at the ^{57}Fe nucleus is low because the spin is only partly centered at iron.

In a recent paper, Wieghardt and co-workers have performed elaborated density functional theory calculations to explain experimental observables including isomer shift, efg, EPR *g* values, and magnetic hyperfine coupling tensors noted for series of comparable non-heme iron nitrosyls.[11a] It is interesting to note that the such data for **2** and **3** can be interpreted in the light of the same arguments. In this framework, the Mössbauer isomer shift values observed for **2** and **3** (Table 4) are most likely due to the influence of the π-acceptor strength of NO^+ (present in **2**) and $NO^\bullet$ (present in **3**). This assumes that in both cases, the iron center is low-spin Fe(II) and it is only the nitrosyl ligand that differs from NO^+ (in the $\{Fe-NO\}^6$ species) to $NO^\bullet$ (in the $\{Fe-NO\}^7$ species). The low spin density at the iron site in **3** corroborates this notion. This assignment is also supported by the small efg tensor in both cases that results in vanishing valence contributions for low-spin Fe(II) due to the $(t_{2g})^6$

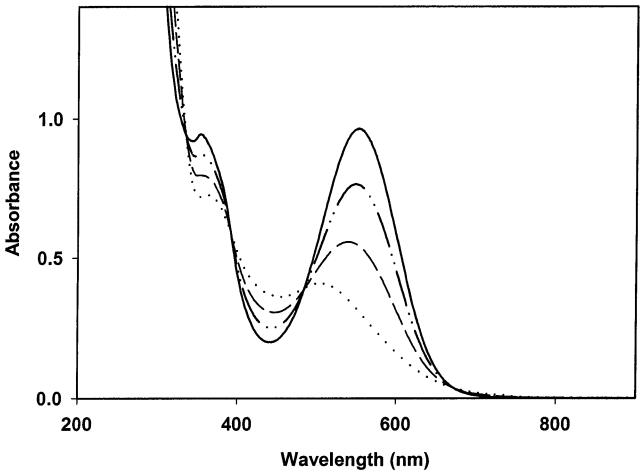

Figure 10. Conversion of $[(PaPy_3)Fe(NO)](ClO_4)_2$ (**2**, dotted line) to $[(PaPy_3)Fe(MeCN)](ClO_4)_2$ (**1**, solid line) in MeCN under illumination with a 50-W tungsten lamp ($t_{1/2}$ = 45 s, concentration of **2** = 0.4 mM).

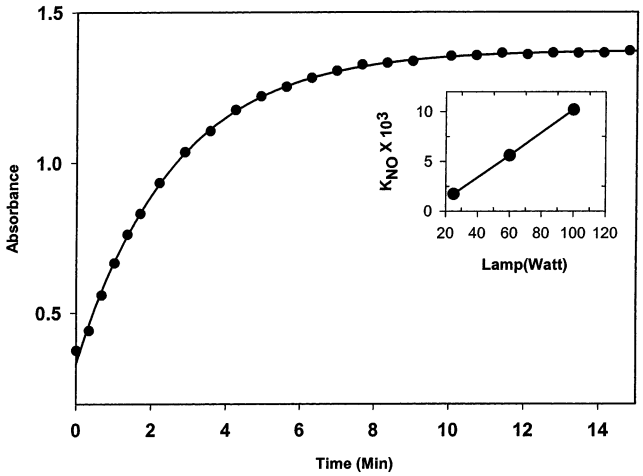

Figure 11. Increase in absorbance at 550 nm of a solution of **2** in MeCN with time upon illumination (60-W tungsten lamp) and the fit to an exponential function. Inset: Plot of K_{NO} values with the light power (in watt). See text for details.

configuration. Since NO^+ is the stronger π acceptor, one expects **2** to exhibit smaller isomer shift and larger quadrupole splitting compared to **3**, which contains NO•.[11a] This is indeed what we observe (Table 4).[33] Finally, the low values of the **A**-tensor and Fermi contact contribution for the ^{57}Fe Mossbauer nucleus of the $\{Fe-NO\}^7$ complex **3** and its fairly isotropic **g** matrix (low spin−orbit coupling) indicate that the spin is predominantly centered on the nitrogen of the bound NO ligand.

Photolability of the Bound NO in 2. In the solid state, **2** is very stable toward light (no decomposition in months). When the red solution of **2** in MeCN is kept in the dark, the electronic absorption spectrum (rapid scan) does not change appreciably even after 48 h (Figure S1, Supporting Information). However, when the cuvette is exposed to light (50 -W tungsten lamp), the color changes rapidly to purple (color of **1**).[17] The changes in the absorption spectrum upon conversion of **2** into **1** under light are shown in Figure 10. The clean conversion of the NO-bound complex **2** into the MeCN-bound species **1** is indicated by the isosbestic points at 484, 392, and 334 nm. It is important to note that no back reaction is observed when the light is turned off. It thus appears that in dilute solution, the solvent-bound species resists re-formation of the nitrosyl complex. However, **2** can be synthesized in the reaction of **1** and excess NO in MeCN and, hence, the binding of NO to the iron center of **2** is *reversible*. Complex **2** is therefore the first non-heme Fe(III) species that binds NO reversibly and exhibits photolability of bound NO under *very mild* conditions. Quite in contrast, the $\{Fe-NO\}^7$ complex **3** does not show any photolability of the bound NO in solid state or in solution.

Table 5. Values of K_{NO} of **2** in Different Solvents under Different Light Intensity

solvent	light intensity (W)	$K_{NO} \times 10^3$ (s^{-1})
MeCN	25	1.73 ± 0.006
	60	5.60 ± 0.014
	100	10.20 ± 0.018
H_2O	25	0.96 ± 0.006
	60	2.41 ± 0.009
	100	3.56 ± 0.007
DMF	25	1.24 ± 0.010
	60	3.78 ± 0.018
	100	5.87 ± 0.012

A pseudo-first-order behavior has been noted in photolysis of **2** (eq 1) in three different solvents (MeCN, DMF, and H_2O). The value of the NO off rate constant, K_{NO}, increases linearly with the intensity of light (Figure 11). In water, the rate of loss of NO is slower than that observed in MeCN

$$[(PaPy_3)Fe(NO)]^{2+} + MeCN \xrightarrow{h\nu} [(PaPy_3)Fe(MeCN)]^{2+} + NO \quad (1)$$

(Table 5). Although the solvated species are stable in the cases of MeCN and H_2O, photolysis studies in DMF indicate that the DMF-bound species is not very stable and decomposition is observed within 30 min. The K_{NO} values of **2** in different solvents (Table 5) are smaller than the K_{off} values of the NO adducts of Fe(III) porphyrins.[5a] However, one must consider the mild photolysis conditions that have been employed in the present work. The fact that simple exposure to ordinary light expels NO from **2** makes this nitrosyl a good candidate for photodynamic therapy. More work is under way to establish this claim at the present time.

Nucleophilic Attack on Coordinated NO in 2. The reactivity of bound NO in metal nitrosyls has been the subject of research for quite sometime.[1,2,5a,34] Coordinated NO is known to be rather inert to displacement by ligands such as

(30) Rohde, J.-U.; In, J.-H.; Lim, M. H.; Brennessel, W. W.; Bukowski, M. R.; Stubna, A.; Münck, E.; Nam, W.; Que, L., Jr. *Science* **2003**, *299*, 1037.
(31) (a) Feltham, R. D.; Enemark, J. H. *Topic in Inorganic and Organometallic Stereochemistry*; Geoffroy, G. L., Ed.; *Topics in Stereochemistry*, Vol. 12; Allinger, N. L., Eliel, E. L., series Eds.; Wiley: New York, 1981; p 155. (b) Westcott, B. L.; Enemark, J. H. In *Inorganic Electronic Structure and Spectroscopy*; Solomon, E. I., Lever, A. B. P., Eds.; Wiley: New York, 1999; Vol. II, p 403.
(32) Feig, A.; Bautista, M. T.; Lippard, S. *J. Inorg. Chem.***1996**, *35*, 6892.
(33) Stronger π acceptance by NO^+ is also indicated by a higher value of the ν_{CO} in the case of **2** (1644 cm^{-1}). The same stretch is noted at 1613 cm^{-1} in the case of **3** that contains NO•. In addition, the N−O distance of **2** is 0.05 Å shorter than the N−O distance of **3**. This fact supports the notion that **2** is best described as $Fe(II)-NO^+$ while an Fe(II)−NO• formulation is more suitable for **3**.

OH^-, CN^-, CO, and tertiary phosphines due to the inherent strength of the M−N(O) bond(s). This facilitates reactions on the coordinated NO.[34] Bottomley and co-workers have suggested that metal nitrosyl complexes with $\nu_{NO} > 1886$ cm^{-1} or better and f(NO) > 13.8 mdyn $Å^{-1}$ will be susceptible to attack at the nitrogen atom by nucleophiles.[35] For example, addition of OH^- to metal nitrosyls like $[Ru(bpy)_2(NO)X]^{2+}$, $[Ru(diars)_2Cl(NO)]^{2+}$ (bpy = 2,2′-bipyridyl; diars = *o*-phenylenebis(dimethyl)arsine), $[Ir(NO)X_5]^{2-}$ (X = halide ions), and $[Os(CN)_5(NO)]^{2-}$ readily affords the corresponding N-bound nitro complexes.[34] However, the only example of OH^- attacking a coordinated NO ligand of a non-heme iron complex reported in the literature is the reaction between OH^- and $[Fe(CN)_5NO]^{2-}$ (eq 2).

$$[Fe(CN)_5NO]^{2-} + 2OH^- \rightleftharpoons [Fe(CN)_5NO_2]^{4-} + H_2O \quad (2)$$

Since **2** displays a strong ν_{NO} stretch at 1919 cm^{-1} and the comparatively short Fe−N(O) bond distance (1.677(2) Å) suggests an appreciable double bond character, one expects the nitrogen of the coordinated NO in **2** to exhibit electrophilic character. Indeed, reaction of **2** with $[Et_4N][OH]$ in MeCN solution in the dark affords the corresponding N-bound nitro complex **4** in high yield according to eq 3.

$$[(PaPy_3)Fe(NO)]^{2+} + OH^- \xrightarrow{O_2} [(PaPy_3)Fe(NO_2)]^+ + H_2O \quad (3)$$

Since reactions of OH^- with heme and non-heme Fe(III) nitrosyls lead to Fe(II)−nitro species[5a] and reaction 3 goes to completion only in the presence of dioxygen, it is evident that the Fe(II)−nitro intermediate formed in the first step of reaction 3 is finally oxidized to **4** by dioxygen. The nucleophilic attack of OH^- to coordinated NO in **2** provides support to the Fe(II)−NO^+ formulation as discussed above.

Electrophilic Attack on Coordinated NO in 3. While the {Fe−NO}^{6} complex **2** is quite insensitive to dioxygen, the {Fe−NO}^{7} complex **3** exhibits high sensitivity to dioxygen particularly when in solution. For example, when a solution of **3** in MeCN is exposed to air, the N-bound nitro complex **4** is rapidly formed in high yield (eq 4).

$$[(PaPy_3)Fe(NO)]^+ + {}^1/_2O_2 \rightarrow [(PaPy_3)Fe(NO_2)]^+ \quad (4)$$

Recently, Richter-Addo and co-workers have reported conversion of a bound NO to N-bound NO_2 upon exposure of a pentacoordinated iron nitrosyl complex of a picket fence porphyrin (tpivpp) to air in the presence of pyridine.[36] According to these researchers, this is the "first unambiguous demonstration of a nitrosyl-to-nitrite conversion in an iron nitrosyl porphyrin". It is important to note that this conversion occurs only in the presence of a base that also acts as the sixth ligand. In **3**, the coordinated carboxamido nitrogen serves this role of base and, hence, exposure of solutions of **3** to dioxygen readily affords the N-bound nitro complex **4**. To our knowledge, this is the first example of a nitrosyl-to-nitrite conversion in a non-heme iron nitrosyl. As discussed above, the EPR data indicate the presence of considerable electron density on the nitrogen of the NO ligand in **3**. The electrophilic attack of dioxygen to the NO in the case of **3** is therefore expected, and once again this reactivity supports the Fe(II)−$NO^•$ formulation of **3**. The mechanisms of the reactions of **2** and **3** with OH^- and O_2, respectively, are under study at the present time.

Role of Carboxamide Moiety. The presence of the carboxamido nitrogen in **2** and **3** has a profound effect on the reactivity of the iron centers in these complexes. This fact becomes evident when one compares the reactivities of **2** (and **3**) with those of the Fe(III) and Fe(II) complexes of the Schiff base $SBPy_3$. These four iron complexes are all low spin and their metric parameters are very similar except for the fact that **2** and **3** contain a carboxamido nitrogen while the $SBPy_3$ complexes contain an imine nitrogen at the same place. As a general rule, polypyridine ligands such as $SBPy_3$ stabilize Fe(II) to a great extent.[19,37] The stabilization is readily evident by the highly positive $E_{1/2}$ values for the Fe(II)/Fe(III) couple of iron complexes of such ligands.[37] In a previous account, we have reported spontaneous reduction of the Fe(III) complex of $SBPy_3$ to the corresponding Fe(II) species in MeCN.[19] Such stable Fe(II) species do not bind NO. Introduction of one carboxamide group into the ligand frame, however, raises the stability of the +3 oxidation state of iron,[18] and as a result the $E_{1/2}$ of $[(PaPy_3)Fe(MeCN)]^{2+}$ (**1**) is noted at +0.21 V (vs SCE), a value 0.8 V lower than the $E_{1/2}$ of $[(SBPy_3)Fe(MeCN)]^{2+}$ (1.01 V vs SCE). This fact allows **1** to bind NO and afford $[(PaPy_3)Fe(NO)]^{2+}$ (**2**). Spectroscopic data, discussed above, suggest an Fe(II)−NO^+ formulation of **2**. It thus appears that the more stabilized Fe(III) center of **1** promotes transfer of the single electron of NO to a more metal-based orbital and increases the affinity between the iron center and NO. We believe that irradiation at a LMCT region weakens this interaction and, hence, NO in **2** is photolabile. NO labilization resulting from population of a dissociative excited state has been reported in the case of [Ru(salen)(Cl)(NO)] by Ford and co-workers.[38] At this time, we are synthesizing more iron complexes of similar kind to prove this mechanism of photolabilization of coordinated NO in iron nitrosyls. Interestingly, both **2** and [Ru(salen)(Cl)(NO)] contain a negatively charged donor trans to the bound NO molecule. The situation is very similar at the iron site in Fe−NHase where a negatively charged thiolato sulfur is trans to the bound NO ligand. Since all three M(III) centers exhibit photolability of the bound NO, it appears that the presence of a negatively charged donor trans to NO could be a requirement for photolability. More studies are however required to confirm this hypothesis.

(34) (a) McCleverty, J. A. *Chem. Rev.* **1979**, *79*, 53. (b) Bottomley, F. *Acc. Chem. Res.* **1978**, *11*, 158.
(35) Bottomley, F.; Brooks, W. V. F.; Clarkson, S. G.; Tong, S.-B. *J. Chem. Soc., Chem. Commun.* **1973**, 919.
(36) Cheng, L.; Powell, D. R.; Khan, M. A.; Richter-Addo, G. B. *Chem. Commun.* **2000**, 2301.
(37) (a) Goldsmith, C. R.; Jonas, R. T.; Stack, T. D. P. *J. Am. Chem. Soc.* **2002**, *124*, 83. (b) Roelfes, G.; Lubben, M.; Chen, K.; Ho, R. Y. N.; Meetsma, A.; Genseberger, S.; Hermant, R. M.; Hage, R.; Mandal, S. K.; Young, V. G., Jr.; Zang, Y.; Kooijmann, H.; Spek, A. L.; Que, L., Jr.; Feringa, B. L. *Inorg. Chem.* **1999**, *38*, 1929.
(38) Works, C. F.; Ford, P. C. *J. Am. Chem. Soc.* **2000**, *122*, 7592.

Summary and Conclusions

The following are the principal findings and conclusions of this investigation:

(i) The iron nitrosyl complexes of $\{Fe-NO\}^6$ and $\{Fe-NO\}^7$ type have been synthesized with a pentadentate ligand $PaPy_3H$. These two iron complexes, namely, $[(PaPy_3)Fe(NO)](ClO_4)_2$ (**2**) and $[(PaPy_3)Fe(NO)](ClO_4)$ (**3**), contain one carboxamido nitrogen in the donor set. The structures of **2**, **3**, and one genuine Fe(III) complex with an "innocent" sixth ligand, namely, $[(PaPy_3)Fe(NO_2)](ClO_4)$ (**4**), have been determined.

(ii) Spectroscopic data for **2** and **3** reveal an $Fe(II)-NO^+$ and $Fe(II)-NO^{\bullet}$ formulation for the $\{Fe-NO\}^6$ (**2**) and $\{Fe-NO\}^7$ (**3**) species, respectively.

(ii) Complex **2** is the first non-heme iron nitrosyl of $\{Fe-NO\}^6$ type where the binding of NO is reversible and the bound NO is photolabile under mild condition (25-W tungsten lamp).

(iii) Complex **2** readily reacts with OH^- in MeCN in the dark to afford the corresponding nitro complex **4**. This nucleophilic attack at the nitrogen center of bound NO supports the $Fe(II)-NO^+$ formulation of **2**.

(iv) Complex **3** is the first non-heme iron nitrosyl complex that reacts rapidly with dioxygen to afford the corresponding nitro complex **4**. The electrophilic attack of dioxygen at the nitrogen center of bound NO supports the $Fe(II)-NO^{\bullet}$ formulation of **3**.

Acknowledgment. Financial support from a NIH grant (GM 61636) is gratefully acknowledged. The Bruker SMART 1000 diffractometer was funded in part by the NSF Instrumentation Grant CHE-9808259.

Supporting Information Available: Electonic absorption spectrum of **2** in MeCN in the dark (Figure S1) and X-ray crystallographic data (in CIF format) and tables for the structure determination of complexes $[(PaPy_3)Fe(NO)](ClO_4)_2$ (**2**·MeCN), $[(PaPy_3)Fe(NO)](ClO_4)$ (**3**·2MeCN), and $[(PaPy_3)Fe(NO_2)](ClO_4)$ (**4**·2MeCN). This material is available free of charge via the Internet at http://pubs.acs.org.

IC0301627